Co^{3+}-O-V^{4+} cluster in CoVOx nanorods for efficient and stable electrochemical oxygen evolution

Chaoran Jiang, Ji Yang, Tingting Zhao, Lunqiao Xiong, Zheng-Xiao Guo, Yujing Ren, Haifeng Qi, Aiqin Wang, and Junwang Tang**

Dr. Chaoran Jiang, Lunqiao Xiong, Prof. Junwang Tang
Department of Chemical Engineering, University College London, Torrington Place, London, WC1E 7JE, UK.
E-mail: junwang.tang@ucl.ac.uk
Dr. Tingting Zhao, Prof. Zheng-Xiao Guo
Department of Chemistry, University College London, 20 Gordon Street, London, WC1H 0AJ, UK.
Department of Chemistry, The University of Hong Kong, Pokfulam Road, Hong Kong; HKU Zhejiang Institute of Research and Innovation, Hangzhou, PR China.
Dr Chaoran Jiang, Ji Yang, Dr. Yujing Ren, Haifeng Qi, Prof. Aiqin Wang
State Key Laboratory of Catalysis, Dalian Institute of Chemical Physics, Chinese Academy of Sciences, Dalian, 116023, China.
E-mail: aiqin.wang@dicp.ac.cn

Keywords: Co^{3+}-O-V^{4+} cluster, nanorods, electrocatalysts, oxygen evolution, stability

The development of cost-efficient and long-term stable catalysts for the oxygen evolution reaction (OER) is crucial to produce clean and sustainable H_2 fuels from water. Here we demonstrate a cobalt vanadium oxide (CoVOx-300) working as such an efficient and durable electrocatalyst. Such an active catalyst is beneficial from the balanced Co^{3+}-O-V^{4+} active species, which show the high surface Co^{3+} contents with matched V^{4+} generated by rapid heat treatment. The CoVOx-300 with highest Co^{3+}/Co^{2+} ratio of 1.4 and corresponding highest V^{4+}/V^{5+} ratio of 1.7 exhibits remarkable OER activity with an overpotential of 330 mV at current density of 10 mA cm^{-2} (η_{10}), a shallow Tafel slope of only 46 mV dec^{-1} and a current density of 100 mA cm^{-2} at an overpotential of 0.38 V vs RHE, which is 20 times higher than the active CoOx-300 and 1000 times higher than VOx-300. The catalyst also shows excellent stability for 10 hours in alkaline media and a 40 % reduced activation energy to the counterpart, CoOx-300. The overpotential (η10) of CoVOx-300 also shows nearly 70 and 80 mV lower than the corresponding CoOx-300 and CoVOx catalysts, respectively and 20 % lower Tafel slope than the commercial benchmark catalyst RuO_2. Thus, this study for the first time demonstrates that

surface Co^{3+}-O-V^{4+} species play a crucial role in improving electrocatalytic properties and stability for water oxidation reaction and the approaches allow the rational design and synthesis of other active transition metal oxides toward efficient OER activity.

Efficient electrochemical water splitting to produce hydrogen fuel has been considered as a promising strategy for renewable energy conversion and storage. In water splitting the sluggish kinetics of the oxygen evolution reaction (OER) is a rate-determining step due to its multi-electron transfer mechanisms ($2H_2O \rightarrow 4H^+ + O_2 + 4e^-$).[1] Efficient OER catalysts are thus required to improve the kinetics and lower the overpotential. State of the art OER catalysts, based on precious metals such as RuO_2, can perform the OER with an overpotential close to 370 mV at a current density of 10 mA/cm^2.[2] However, the scarcity and cost of those metals limit their large-scale applications. The use of low-cost catalysts, especially the 3d metal (V, Mn, Fe, Co, Ni) compounds, has shown great potential to replace the highly active but scarce noble metal oxides (e.g., IrO_2 and RuO_2).

Cobalt-based electrocatalysts have been studied as promising OER candidates because of their excellent charge transport properties.[3] To date, several effective strategies have been employed to improve the OER performance. For example, Xu et al reported a composite with Co single atoms anchored on Co_3O_4 and nitrogen-doped active carbon (Co- Co_3O_4@NAC). The highly dispersed Co atoms and Co_3O_4 on NAC lead to abundant active sites, resulting in a OER performance with an overpotential of 1.61 V (vs RHE) at 10 mA/cm^2.[4] Zhang et al found that sulfurization and cation modulation of cobalt hydroxide could effectively alter the electronic properties of Co, leading to a unique $Co_3FeS_{1.5}(OH)_6$ electrocatalyst with 10 mA/cm^2 OER current density at 1.588 V (RHE).[5] In fact, other previous studies have demonstrated that the proper control of Co electronic structure or the Co^{3+}/ Co^{2+} ratio in the Co_3O_4 could lead to significant modifications on its electrocatalytic properties.[6] Sun et al. found that the surface

Co^{3+} species of Co_3O_4 crystal were the active sites of OER,[7] which was further proved by Dai et al. through X-ray absorption near-edge spectrum (XANES) observations.[8] The higher Co^{3+}/Co^{2+} ratio is favourable for creating more targeted *OOH intermediates, which is beneficial for boosting OER activity.[9] Therefore, diverse approaches were developed to achieve a high concentration of Co^{3+}, such as high-temperature calcination,[10] coating with an oxidant,[11] meal ion insertion[12] and introducing highly electronegative support.[13] On the other hand, through Ar plasma[6], NH_3 plasma[14] or $NaBH_4$[15] solution treatment, the lower atomic ratio of Co^{3+}/Co^{2+} in Co_3O_4 could be achieved, which was believed to be indicative of relatively more oxygen vacancies.[16] These oxygen vacancies near the Co^{3+} could improve electronic conductivity and facilitate adsorption of H_2O onto nearby Co^{3+} sites.[16]

To understand the two conflicting conclusions, we attempted to manipulate the Co^{3+}/Co^{2+} ratio on the surface of cobalt oxides To date, tuning the surface Co^{3+}/Co^{2+} ratio or electronic structure through doping other transition-metal elements such as Ni, Fe, Mo, Mn, Zn and, Al, into cobalt based material to form bimetallic oxide/hydroxide catalyst has proved to be an effective way for efficient water splitting.[17] In particular, Yan et al. found that Co^{3+}/Co^{2+} ratio of $Co_{3-x}AlxO_4$ could be controlled by varying Al^{3+} dopant concentration[18] and Xing et al. reported the high stability of zinc-doped $NiCo_2O_4$ electrode resulted from the stabilisation of Co^{3+} in the presence of Zn.[19] Moreover, vanadium (V^{3+} and V^{4+}) dopant level has been shown to have a substantial effect on Fe^{3+}/Fe^{2+} ratio in the magnetite for water gas shift reaction,[20] and very recently Sun et al has proved that vanadium incorporation into iron oxyhydroxide could effectively lower the overpotential of water oxidation due to the excellent conductivity, facile electron transfer and abundant active sites of oxyhydroxide.[21]

Inspired by these findings, for the first time, we report here a reproducible strategy of incorporating vanadium into CoOx nanorods and subsequent rapid heat treatment to produce Co^{3+}-O-V^{4+} in the CoVOx nanorod catalysts (noted as CoVOx-300). In combination with

various characterizations, we have demonstrated the synergistic effect between Co^{3+} and V^{4+} for efficient water oxidation, which was achieved by controlling the ratio of V^{4+} to V^{5+} on CoVOx-300 surface, leading to 20 times higher current than CoOx-300 without V^{4+} at the identical overpotential of 0.38 V. Such understanding of the structure-activity relationship for electrocatalytic reactions demonstrated on CoVOx-based catalysts could be applied to other candidate electrocatalysts.

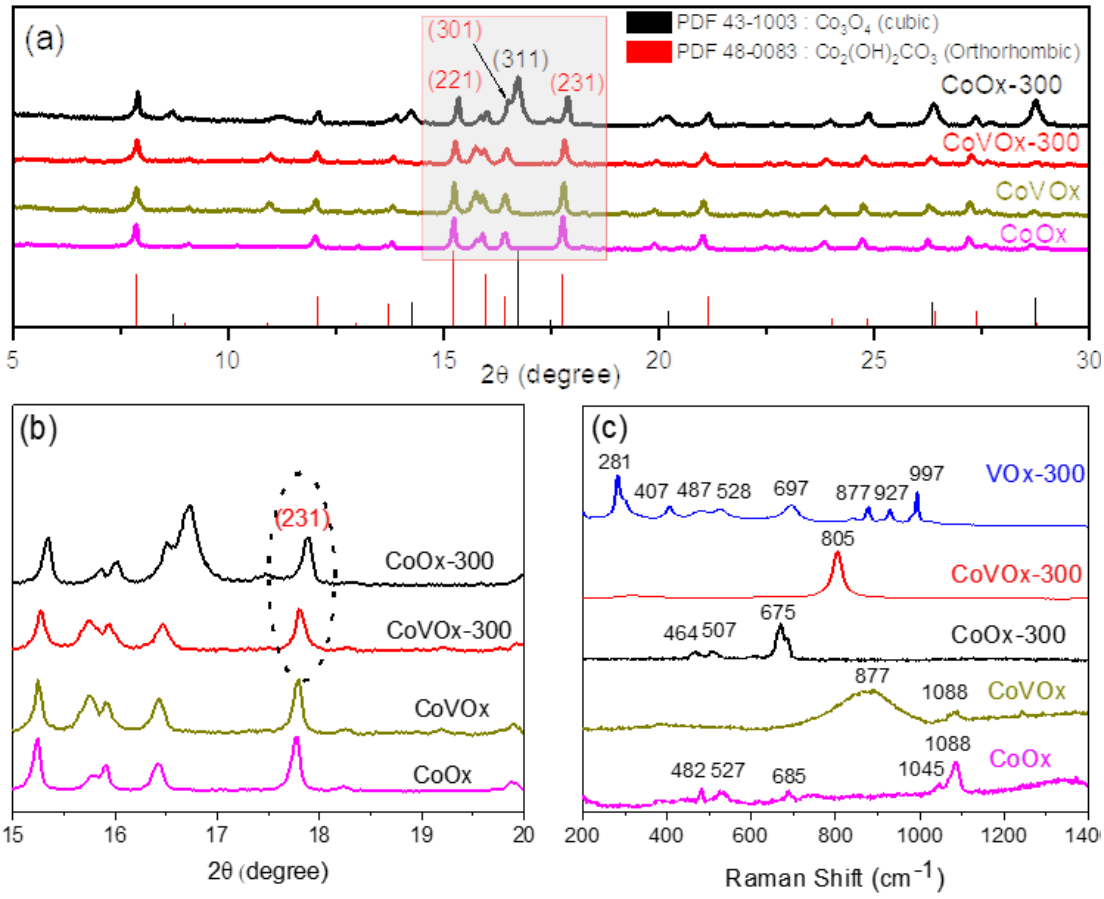

Figure 1. (a) XRD patterns of CoOx, CoVOx, CoOx-300 and CoVOx-300 with standard JCPDS card number 48-0083 and 43-1003. (b) Enlarged view of the corresponding XRD patterns at the range of 2θ between 15 and 20 degree. (c) Raman spectra of CoOx, CoVOx, VOx-300, CoOx-300 and CoVOx-300.

Hydrothermal synthesis was used to produce CoOx, VOx and CoVOx catalysts (see

experimental section in supporting information for details). The as-synthesized samples were further processed by rapid heat treatment in air at 300 ℃ for 5 mins, and these were noted as CoOx-300, VOx-300 and CoVOx-300, respectively. The composition and crystallinity of all the samples were analysed by XRD (Figure 1 & S1). As shown in Figure 1a, apart from CoOx-300, the diffraction peaks of other three samples can be well indexed to a pure cobalt hydroxide carbonate phase with orthorhombic structure ($Co_2(OH)_2CO_3$, JSPDS 48-0083) while some Co was replaced by V in the structure.[22] Based on the experimental condition, we denoted as the three samples CoOx, CoVOx, and CoVOx-300 herein with the detail in the experimental section. In comparison with CoVOx-300, the cobalt phases of CoOx-300 is partially crystallized to cubic-phase spinel Co_3O_4 (JCPDS card no.43-1003),[23] which results in a mixed cobalt phase ($Co_2(OH)_2CO_3$ and Co_3O_4). This suggests the strong interaction between cobalt and vanadium suppresses structure change of CoVOx, and thus CoVOx-300 could preserve the crystal orthorhombic structure. The diffraction peaks of VOx and VOx-300 can be assigned to $VO(OH)_2$ (JCPDS 11-0209) and V_2O_5 (JCPDS card no. 001-0359), respectively, according to previous literature (Figure S1a).[24] Noticed that no VOx species could be identified in the sample of CoVOx and CoVOx-300, suggesting the great possibilities that vanadium incorporation into CoVOx or CoVOx-300. Furthermore, the enlarged XRD patterns of the above samples (Figure 1b) show that there is a slight shift in (231) diffraction peak toward lower two-theta value when introducing vanadium into CoOx lattice. The oxygen vacancies and lattice distortion due to the vanadium incorporation are the essential reasons for the shift in XRD pattern towards low two theta. The shift is much more apparent when comparing CoVOx-300 and CoOx-300, which indicates that the rapid heat treatment promotes the vanadium incorporation. However, upon the heat treatment of CoVOx sample at either high temperature for a short period (600 °C/5mins) or low temperature for an extended period (300 °C/2 h), the CoVOx samples were oxidized to cubic-phase spinel Co_3O_4 (JCPDS card no.43-

1003),[23] which were noted as CoVOx-600 and CoVOx-300 (2 h) in Figure S1b, respectively.

Figure 1c shows Raman spectra of CoOx, CoVOx, VOx, CoOx-300 and CoVOx-300 and VOx-300. CoOx sample can be identified as cobalt hydroxy carbonate in the 800–1400 cm^{-1} region, which is characterised by an intense sharp peak at 1088 cm^{-1}. This band is assigned to the ν1 CO_3^{2-} symmetric stretching mode. The shoulder at 1045 cm^{-1} is assigned to a hydroxyl deformation mode.[25] Other Raman bands observed at 482, 527 and 685 are attributed to Co-O E_g, F_{2g} and A_{1g} variation modes, respectively. Whereas, upon rapid heat treatment at 300 °C for 5 min, CoOx-300 exhibits four characteristic peaks located at 464, 507, 606, and 675 cm−1, which correspond to E_g, F_{2g}^1, F_{2g}^2, and A_g^1 modes of the Co_3O_4 crystal.[26] VOx-300 exhibits four distinct peaks located at 281,407,697 and 997 cm^{-1}, similar to the characteristic peaks of reported lepidocrocite VOOH sphere.[27] In detail, the first two peak at 281 and 407 cm-1 are assigned to the bending vibration of the V =O bonds.[28] The peak at 697 cm^{-1} is assigned to the doubly coordinated oxygen (V_2–O) stretching mode which results from corner-shared oxygens.[28] The relative sharp peak at 997 cm^{-1} corresponds to the stretching mode of vanadyl oxygen (V-O).[28] The two weak peaks at 487 and 528 cm^{-1} are assigned to the bending vibrations of bridging V-O-V (double coordinated oxygen) and triple coordinated oxygen (V_3–O) stretching mode, respectively.[28] Also, there is a peak at 927 cm^{-1}, which is attribute to V^{4+}= O bond.[29] The peak at 877 cm^{-1} is assigned to the ν1 symmetric stretching mode of VO_4.[30] The CoVOx sample preserves the ν1 CO_3^{2-} symmetric stretching mode at 1088 cm^{-1} and exhibits a broad peak centred at 877 cm^{-1}, which could be tentatively explained in terms of stretching mode of VO_4 tetrahedral with A1. The cobalt cations may be bonded with each oxygen atom of a VO_4 tetrahedral to form Co-O-V-O species. This may introduce some asymmetry in the VO_4 unit without disturbing the overall cubic symmetry of the elementary unit cell.[31] Similar features of Raman modes are observed on reported $LiCoVO_4$.[31] However, Raman bands corresponding to either V-O or Co-O vibration modes are not observed in

CoVOx-300 sample. The sharp peak at 805 cm^{-1} situated between Co-O A_g^1 (675 cm^{-1}) and VO_4 A1 mode, is very likely due to the variation mode of Co-O-V. Further, the strong peak at 1088 cm^{-1} disappears due to decomposition of carbonates after rapid heat treatment. This result indicates the rapid heat treatment not only increases the crystallinity of the CoVOx but also generate Co-O-V species, probably due to the intense interaction between cobalt and vanadium, supported by the H_2-TPR profile (Figure S2), which was used to observe the reducibility of catalysts. There are three peaks (at 320, 390, and 415 ℃) in the H_2-TPR profile of CoOx-300 which is composed of both Co_3O_4 and cobalt hydroxide carbonate as mentioned above. There are three peaks (at 320, 390, and 415 ℃) in the H_2-TPR profile of CoOx-300. The two peaks at 320 ℃ and 390 ℃ can be attributed to two-step reduction of Co_3O_4 (Co^{3+}) to CoO (Co^{2+}) and subsequently to Co, respectively.[32] The third peak at 415 ℃ in the high temperature side of the second peaks（T_{390}）very likely corresponds to the reduction of bulk cobalt hydroxide carbonate to cobalt metal.[32a] The H_2-TPR profile of the VOx-300 catalyst entails a single reduction peak with the maximum at 560 ℃ due to the reduction of V^{5+}/V^{4+} to V^{3+} in the bulk of VOx-300.[33] The CoVOx-300 shows four typical reduction peaks in the H_2-TPR profile. The two peaks at 300 ℃ and 435 ℃ can be attributed to two-step reduction of Co^{3+} to Co^{2+} and subsequently to Co, respectively. The other two peaks at 475 and 580 ℃ in the high temperature side correspond to the reduction of V^{5+} to V^{4+} and V^{5+}/V^{4+} to V^{3+}, respectively.[34] Noticeably, extra vanadium reduction peak at 475℃ in lower temperature range is observed for CoVOx-300 sample , whereas its Co^{2+} to Co reduction peaks shift to higher temperature compared to the reference samples (VOx-300 and CoOx-300), indicating the strong interaction between cobalt and vanadium ions.[35]

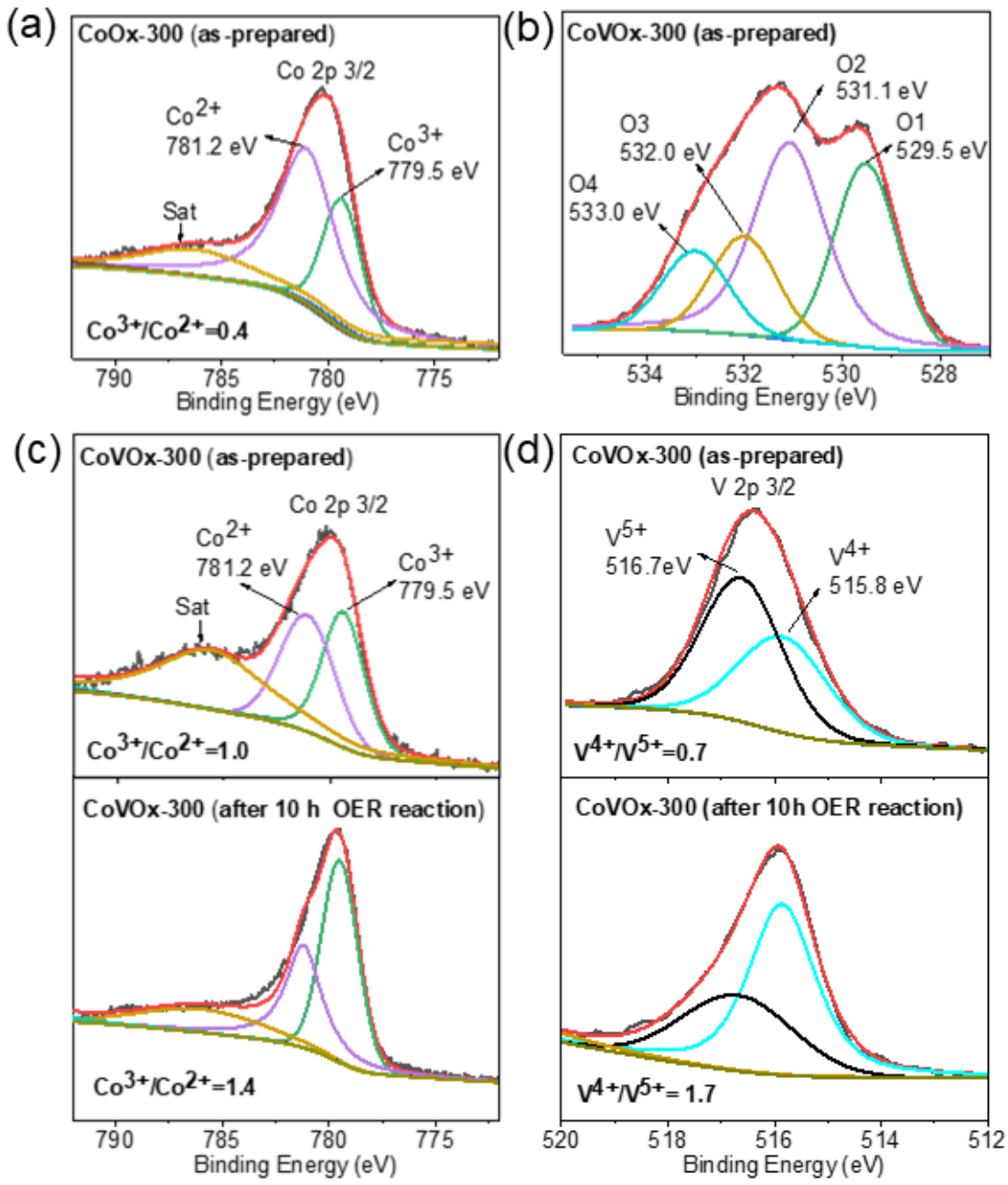

Figure 2. (a): XPS spectra of Co 2p 3/2 for CoOx-300. (b-d) XPS spectra of CoVOx-300: (b) O1s. (c) Co 2p 3/2 for the as-prepared samples and after activation. (d) V 2p 3/2 for the as-prepared samples and after activation. O1, O2, O3 and O4 corresponds to the oxygen atoms bound to metals (529.5 eV), defect sites (531.1 eV), hydroxyl species (532.0 eV) and absorbed molecular water (533.0 eV), respectively.

X-ray photoelectron spectroscopy (XPS) was used to analyse the electronic structure and the

surface composition of the constituents. The core level spectra of the two samples before rapid heat treatment (CoOx and CoVOx) show only the characteristic peak of Co^{2+} at a binding energy of 781.2 eV (Figure S3 a &b). After rapid heat treatment, both CoOx-300 and CoVOx-300 display two major peaks with binding energy at 779.5 and 781.2 eV corresponding to Co^{3+} and Co^{2+}, respectively (Figure 2 a & c), suggesting the coexistence of Co^{3+} and Co^{2+}.[17a, 36] It should be noted that the surface atomic ratio of Co3+/Co2+ for CoOx-300 is 0.4. The Co^{3+}/Co^{2+} ratio is increased to 1.0 for as-prepared CoVOx-300 because of the bigger electronegativity of vanadium ions. Further high Co^{3+}/Co^{2+} ratio of 1.4 is observed for CoVOx-300 after 10 hours' electrochemical reaction due to the in-situ oxidation of cobalt ions under a positive bias (Figure 2c and Figure S8). To investigate the effect of V in CoVOx-300 sample, the XPS spectra of V 2p 3/2 for as-prepared and after electrochemical activation CoVOx-300 samples are compared (Figure 2d). The as-prepared CoVOx-300 exhibit two characteristic peaks corresponding to V^{5+} (516.7 eV) and V^{4+}(515.8eV),[37] respectively, with a V^{4+}/V^{5+} ratio of 0.7. The V^{4+}/V^{5+} ratio is increased from 0.7 to 1.7 after electrochemical activation may due to the electron transfer from cobalt ions to vanadium ions through the oxo bridge The increased Co^{3+}/Co^{2+} well matches with the decreased V^{5+}/V^{4+}, suggesting that the valance states of surface vanadium species in CoVOx-300 play a key role for manipulating the surface Co^{3+}/Co^{2+} ratio. Therefore, one can conclude that the higher ratio of V^{4+}/V^{5+} is favourable for a higher concentration of Co^{3+} and consequently only Co^{2+} is observed when the V^{4+}/V^{5+} ratio is as low as 0.3 for CoVOx (Figure S3).

Moreover, the XPS depth profile analysis of CoVOx-300 reveals that both Co and V ions tend to be at high valence states on the surface, but low valence states in the bulk as discussed in the Supporting Information (Figure S4 & S5). Furthermore, we found that the Co/V ratio changes from 2.9 on CoVOx-300 surface to 4.5 in bulk referring to the XPS survey spectra (Figure S6), which means that vanadium atoms are extremely rich on the surface of CoVOx-

300. Such V^{4+}/V^{5+} rich surface guarantees the high concertation of Co^{3+} on the surface which would boost OER activity.[38] The O1s core level spectra of CoVOx-300 could be fitted and deconvoluted into four characteristic peaks of oxygen atoms bound to metals (529.5 eV for O1), defect sites (531.1 eV for O2), hydroxyl species (532.0 eV for O3) and absorbed molecular water (533.0 eV for O4) (Figure S7).[16]

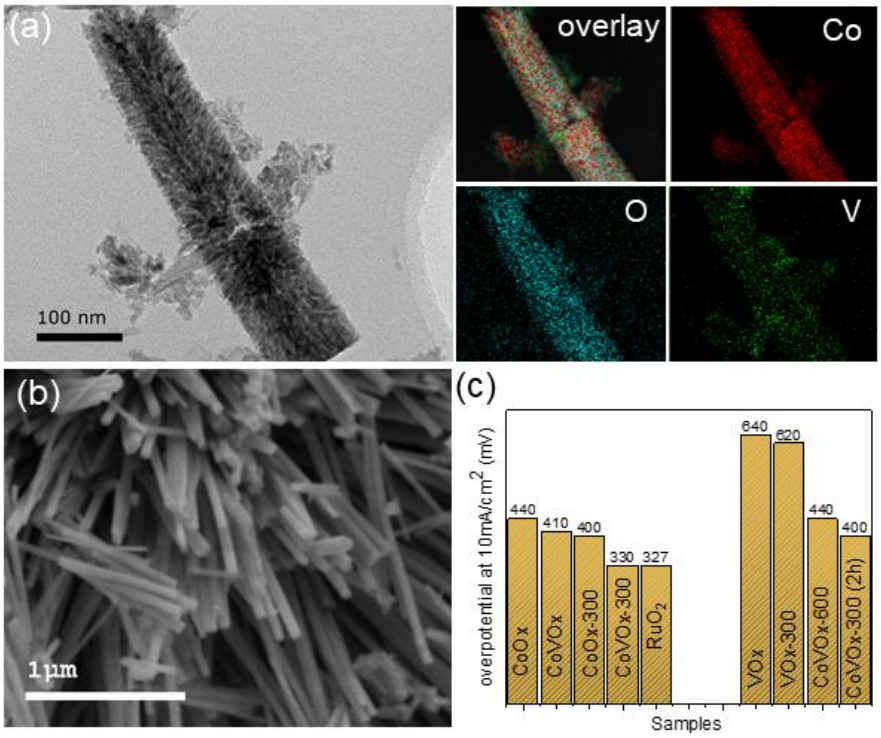

Figure 3. (a): Typical TEM images of CoVOx-300 and the corresponding EDX elemental mapping of cobalt, vanadium and oxygen. (b): Typical SEM image of CoVOx-300 nanorods; (c) The overpotential graph of all studied catalysts.

Typical scanning electron microscopy (SEM) and transmission electron microscopy (TEM) of the CoVOx-300 show nanorod morphology of CoVOx-300 sample (Figure 3). The average diameter of the nanorods is measured to be 80 nm from the TEM image and the cobalt and vanadium species are uniformly distributed over the entire catalyst according to the corresponding EDX elemental mapping images. Furthermore, the HRTEM and the selected

area electron diffraction in Figure S9 indicates that CoVOx-300 nanorods are polycrystalline and display two crystal planes: (221) and (301) of the cobalt carbonate hydroxide.

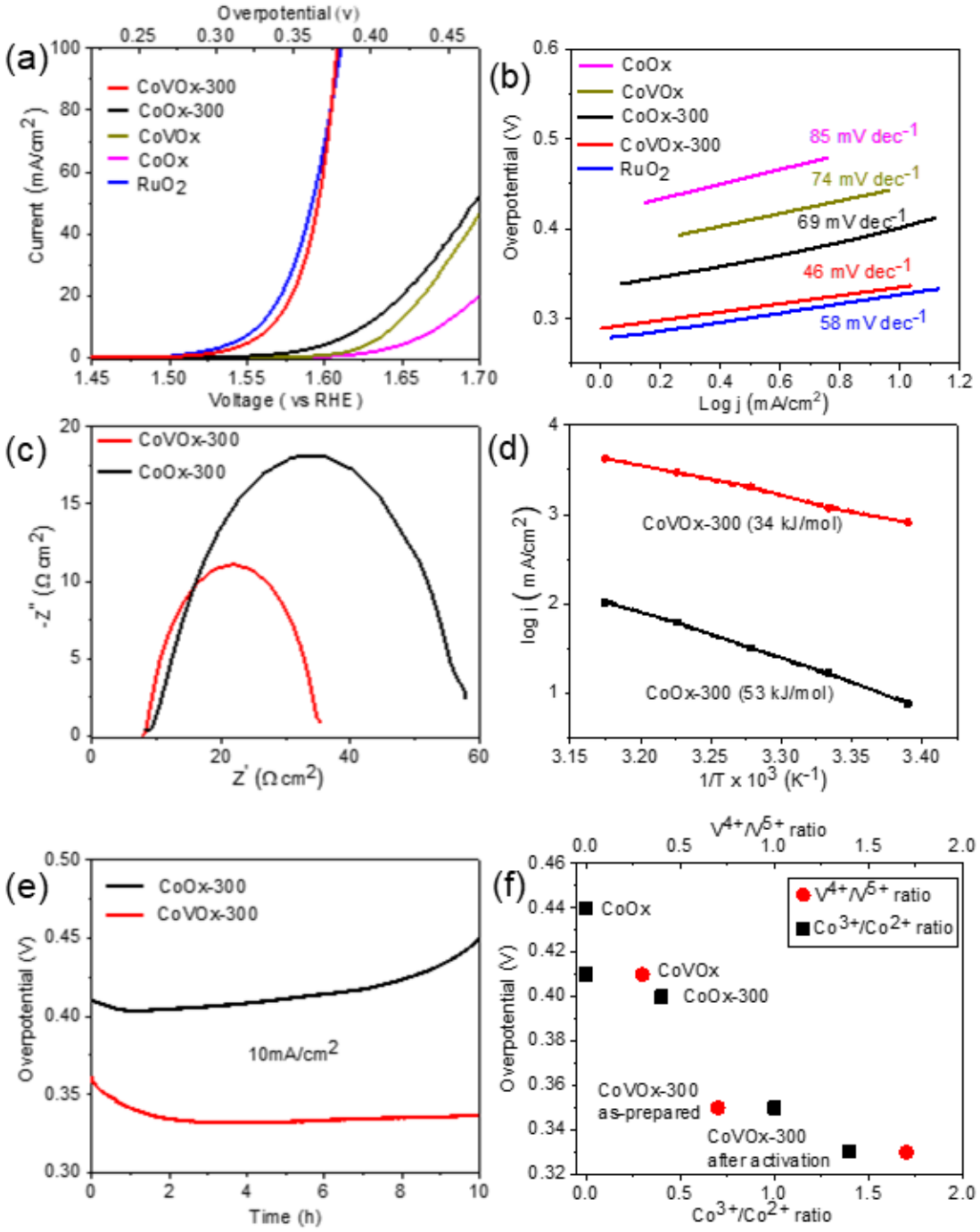

Figure 4. (a): IR corrected LSV curves of CoOx, CoVOx, CoOx-300, CoVOx-300 and commercial RuO_2 at 2 mV/s and 1600 rmp in 1M KOH at 300 K. (b) Tafel plots derived from the polarization curves. (c) Electrochemical impedance spectra measured at an overpotential

of 350 mV at 300 K. (d) Arrhenius plots of the exchange current density J against the inverse temperature 1/T of CoOx-300 and CoVOx-300 at the overpotential of 350 mV. (e) Chronopotentiometric measurements at j = 10 mA/cm2 in 1M KOH for CoVOx-300 and CoOx-300. (f) the trend of overpotentials at j = 10 mA/cm2 with increasing Co^{3+}/Co^{2+} and matched V^{4+}/V^{5+} ratio.

The water oxidation activities of CoVOx prepared with different molar ratios (5:1, 3:1, 1:1, 1:3 and 1:5) of cobalt and vanadium in the precursors were assessed on a glassy carbon electrode in O_2-saturate 1M KOH electrolyte to simulate conditions in a real electrolyser (see experimental details). All the measurements were carried out with ohmic-drop correction and all the amount of the catalyst loadings on GC electrodes were identical at 0.14 mg cm^{-2} for comparison. The electrocatalytic activities are strongly related to the Co/V ratio in CoVOx and increasing Co or decreasing V in the precursors leads to an increase of current (Figure S10a). The best water oxidation performance has been achieved when the molar ratio of Co/V is 3:1. Further increasing the Co reduces the performance likely due to the reduced synergy between Co and V effects. Of note, the influence of the cobalt precursors on the electrocatalytic activity of the CoVOx catalysts with the optimum ratio of Co to V is relatively small (Figure S10b) and $CoCl_2$ was employed in our subsequent studies as it is the best one. The CoVOx (molar ratio of Co/V = 3/1) exhibits a relatively good performance for OER with the overpotential of 410 mV at current density of 10 mA/cm^2 (η_{10} = 410 mV), while the bare CoOx (η_{10} = 440 mV) and VOx (η10 = 640 mV) display poor performance for OER in Figure 4a & S10c, respectively, which is attributed to the synergy between Co and V ions. Interestingly, electrocatalytic activity of both CoVOx and CoOx can be dramatically enhanced by rapid heat treatment in air at 300 °C for 5 mins (noted as CoVOx-300 and CoOx-300 in Figure 4a). The CoOx-300 catalyst requires an overpotential of 400 mV at j =10 mA/cm^2 while it is 330 mV for CoVOx-300 due to increasing Co^{3+} in the two samples (Figure 4f), which is also considerably smaller than 410

mV for untreated CoVOx and 620 mV for VOx-300 (Figure 4a & S10c). Furthermore, it is found that to control the temperature and time is important during the heat treatment of CoVOx. Either rapid heat treatment at 600 ℃ for 5mins (CoVOx-600) or annealing at 300 ℃ for 2 hours (CoVOx-300-2h) would dramatically decrease the catalytic activity and the required overpotentials are 425 mV and 385 mV to drive current of 10 mA/cm^2, respectively (Figure S10d). This may be attributed to the phase change from CoVOx hydroxide to Co_3O_4, supported by the XRD pattern in Figure S1. Therefore, the heat treatment condition is selected as "300 ℃, 5 mins", which not only increases the surface Co^{3+} species, but also holds the original cobalt hydroxide carbonate phase. Previous studies have concluded that oxygen electrocatalysis on meal oxides began with protonation of the surface metal centres to form M-OH.[39] The higher performance of CoVOx-300 than both CoVOx-600 and CoVOx-300-2h could possibly be due to the fast OER kinetics of M-OH than M-O.[40] The lowest η value at 10 mA/cm^2 (η_{10} = 330 mV) highlights the high OER catalytic activity of CoVOx-300, which is comparable with the commercial RuO_2 (Figure 4a) and superior to other six cobalt/vanadium based catalysts investigated here (Figure 3c). Additionally, the overpotential for CoVOx-300 is smaller than other cobalt-based catalysts reported, such as $Co_2V_2O_7$ (η_{10} = 340 mV),[41] $Co_3V_2O_8$ (η_{10} = 359 mV),[42] $Co_3V_2O_8$ nanoroses (η_{10} = 391 mV),[43] and recently reported amorphous CoVOx (η_{10} = 347 mV)[44] tested on a flat glassy carbon electrode in 1M KOH electrolyte.

It has been widely reported that the valence of cobalt ions plays a crucial role in OER catalytic activities and Co^{3+} atoms with intermediate spin in the octahedral and square pyramidal symmetry could be considered as the active sites for OER due to its lower coordination number and large adsorption energy for H_2O molecules, [12, 45] thus promoting to deprotonation of the OOH species to form O_2.[46] In addition, Co^{3+} species can enhance the electrophilicity of materials, promoting the OER process.[13, 46a] Moreover, it has been reported that the OER activity of cobalt hydroxide nanosheets can be improved through doping Fe

atoms.[47] This improvement can be attributed to a change in the OH^- absorption energy difference (ΔG_O-ΔG_{OH}) at the Co sites, and can be rationalized by the difference in electron affinity between Co and Fe ions. Furthermore, Sun's group demonstrated that doping V into FeOOH could dramatically increase the binding energy of *OH and *OOH, leading to a decreased overpotential for OER.[19] Similarly, in our system, the doping of V atoms may also lead to a change in ΔG_{OH} and ΔG_O-ΔG_{OH} at the Co sites, and facilitate the formation of OH^- and O^{2-} on the surface Co^{3+}, promoting the oxidation of Co^{3+} to Co^{4+}. As discussed above (Figure 2), it is shown that higher Co^{3+}/Co^{2+} ratio exists on the surface of CoVOx-300 than that of CoOx-300 catalyst. The results suggest that the vanadium incorporation into CoOx and rapid heat treatment could effectively promote the high concentration of Co^{3+} as the active sites, leading to high OER performance.

The Tafel plot is an inherent method of measuring the catalytic kinetics for the comparative catalysts by fitting the Tafel equation (η=b log j+ a, where η is the overpotential, j is the current density, and b is the Tafel slope). Figure 4b manifests that the Tafel slope of CoVOx-300 (46 mV dec^{-1}) is considerably smaller than that of CoOx-300 (69 mV dec^{-1}), CoVOx (74 mV dec^{-1}), CoOx (85 mV dec^{-1}) and even commercial RuO_2 (58 mV dec^{-1}) when using the same amount catalyst on the electrode. The smallest Tafel slope of CoVOx-300 indicates that the synergetic effect of Co^{3+} and V^{4+} plays a vital role in facilitating the kinetics of OER and enhancing the intrinsic activity. It is interesting to see that among all Co-based OER catalysts (Table S1), the values of the onset potential and overpotential at 10 mV/cm^2 of CoVOx-300 catalyst outperform other reported non-precious OER catalysts tested under comparable conditions. Taking into account all three critical parameters, the onset potential, overpotential at 10 mV/cm^2 and Tafel slope, the CoVOx-300 is the best.

The kinetics of electrode interface reactions were also studied by the Electrochemical Impedance Spectroscopy (EIS) for all the relevant samples (Figure 4c). EIS study of the as-

prepared electrodes was carried out in a three-electrode configuration cell in 1M KOH at 300 K with the overpotential of 350 mV. The Nyquist diagrams of all catalysts show an apparent semicircle, which could be mainly associated with charge transfer resistance (Rct) of the prepared catalysts. CoVOx-300 exhibits lower Rct of 37 Ω cm^2, which is nearly half value of CoOx-300 (60 Ω cm^2), suggesting its superior conductivity and efficient charge transfer. As known, the Ni or Co hydroxide is close to the insulator,[48] resulting in slow kinetics during the OER process. Considering the partially filled d-orbitals of vanadium cations, which may behave like electron acceptor sites, it provides states to accept electrons from the interacting molecules such as CoOx in our case.[49] The high valence vanadium ions incorporation into CoOx lattice facilitates the charge transfer process, which accounts for the improved conductivity, in good agreement with lower Tafel slope in Fig 4b. This is also consistent with the reported V doped Ni(oxy)hydroxide systems, where the V doping induced finite DOS for the spin-down state near the Fermi Level and thus help improve the electrical conductivity of the material.[50]

The temperature-dependent rate data were used to construct Arrhenius plots to obtain the apparent activation energy to compare the intrinsic activities of these catalysts. From the Arrhenius plot as shown in Figure 4d, the apparent activation energy of CoVOx-300 is calculated to be 34 kJ mol^{-1}, *ca.* 40 % smaller than that of CoOx-300 (53 kJ mol^{-1}). This observation indicates that the activity improvement mostly originated from the enhancement of intrinsic activity and the change of associated rate-determining steps. The apparent activation energy value of 34 kJ mol^{-1} for CoVOx-300 compares favourably to other Co-based catalysts such as Fe doped CoP (39.6 kJ mol^{-1}).[51]

The long-term performance or stability is another significant criterion to evaluate an electrocatalyst, especially for commercial applications. To assess the durability of the CoVOx-300 in an alkaline environment, long-term chronopotentiometric experiments at a constant

current density j of 10 mA/cm^2 was performed in O_2-saturated 1M KOH solution at 300 K for 10 h. As shown in Figure 4e, at the initial stage of two hours, the overpotential continues decreasing from 360 mV to 330 mV, owing to an increase of Co^{3+} concentration during the electrochemical activation of the CoVOx-300 electrocatalyst as proved by Figure 2 c and d. After the activation stage, the optimal overpotential of 330 mV has been achieved and remains almost constant towards the end of measurements (10 h), suggesting the excellent stability. In contrast, apart from the initial activation stage, the counterpart CoOx-300 exhibits worse stability as the overpotential keeps increasing toward up to 450 mV after 10 h OER reaction. The outstanding physical and chemical stability of CoVOx-300 was also confirmed by XRD analysis of the CoVOx-300 electrocatalyst before and after 10 h OER reaction (Figure S11). As a result, no phase change is observed. Furthermore, the STEM image and the corresponding mapping images (Figure S12) confirms that the nanorods morphology of the CoVOx-300 is well preserved after 10 h OER reaction, and the Co, V and O elements remain evenly distributed throughout the whole nanorod with some K residue from the electrolyte. This again proves the synergy between Co^{3+} and V^{4+} is the core for the excellent stability and efficient activity.

We further investigated the trend of overpotentials at j = 10 mA/cm^2 with changing Co^{3+}/Co^{2+} and corresponding V^{4+}/V^{5+} ratio on all catalysts. As shown in Figure 4f, the Co^{3+}/Co^{2+} ratio could be easily manipulated by introducing the V^{4+}/V^{5+} couple. With increasing Co^{3+}/Co^{2+} ratio, V^{4+}/V^{5+} ratio increases and then the overpotential decreases. The outstanding activity and stability of CoVOx-300 under alkaline condition thus results from the stabilisation of Co^{3+} active sites by the presence of V^{4+}, indicating the active sites of Co^{3+}-O-V^{4+}.

In summary, a high-performance cobalt vanadium oxide (CoVOx-300) electrocatalyst towards OER has been developed through a two-step method. The vanadium can be homogeneously doped at the surface of cobalt oxides via a reproducible hydrothermal method

followed by a rapid heat treatment. The Co^{3+}/Co^{2+} ratio can be tuned by controlling the V^{4+}/V^{5+} ratio. Our study reveals that increasing V^{4+}/V^{5+} ratio matches with the increased Co^{3+}/Co^{2+} ratio, keeping an overall balanced charge at the surface of the new catalyst, resulting in the highest Co^{3+}/Co^{2+} ratio of 1.4 when the V^{4+}/V^{5+} ratio is tuned up to 1.7 for the CoVOx-300 catalyst. Further studies confirm that the excellent performance of CoVOx-300 is well related to the population of Co^{3+} on the surface, leading to good conductivity and easy electron transfer in the CoVOx-300 catalyst. On a flat glassy carbon electrode, the catalyst reaches 10 mA cm^{-2} at an overpotential of 330 mV in 1M KOH electrolyte with a Tafel slope as low as 46 mV dec^{-1}, 20 % lower than the benchmark commercial electrocatalyst RuO_2. A high density of Co^{3+}-O-V^{4+} formed on the surface of CoVOx-300 is considered as the real active and stable species for OER, which is beneficial to speed up water oxidation and reduce the activation energy for OER by *ca.* 40 % to the CoOx-300 catalyst. The comprehensive investigation of the surface structure-activity relationships for OER paves the way for the design of other transition metal oxides as the low-cost, efficient and stable electrocatalysts for the advanced electrochemical application.

Supporting Information
Supporting Information is available from the Wiley Online Library or from the author.

Conflict of Interest
The authors declare no conflict of interest.

Acknowledgements
C.J. is thankful for financial support from the China Scholarship Council (CSC File NO. 201308060090). C.J. and J.T acknowledge funding from EPSRC (EP/S018204/2/1), Leverhulme Trust (Grant No: RPG-2017-122) and Newton Advanced Fellowship grant ((NA170422 and NAF\R1\191163).

Received: ((will be filled in by the editorial staff))
Revised: ((will be filled in by the editorial staff))
Published online: ((will be filled in by the editorial staff))

[1] J. Tang, J. R. Durrant, D. R. Klug, *Journal of the American Chemical Society* **2008**, *130*, 13885-13891.
[2] F. Guo, H. Yang, L. Liu, Y. Han, A. M. Al-Enizi, A. Nafady, P. E. Kruger, S. G. Telfer, S. Ma, *Journal of Materials Chemistry A* **2019**, *7*, 3624-3631.
[3] X. Zhang, R. Liu, Y. Zang, G. Liu, G. Wang, Y. Zhang, H. Zhang, H. Zhao, *Chemical Communications* **2016**, *52*, 5946-5949.
[4] X. Zhong, W. Yi, Y. Qu, L. Zhang, H. Bai, Y. Zhu, J. Wan, S. Chen, M. Yang, L. Huang, M. Gu, H. Pan, B. Xu, *Applied Catalysis B: Environmental* **2020**, *260*, 118188.
[5] H.-F. Wang, C. Tang, B. Wang, B.-Q. Li, Q. Zhang, *Advanced Materials* **2017**, *29*, 1702327.
[6] L. Xu, Q. Jiang, Z. Xiao, X. Li, J. Huo, S. Wang, L. Dai, *Angewandte Chemie International Edition* **2016**, *55*, 5277-5281.
[7] Y. Zhang, F. Ding, C. Deng, S. Zhen, X. Li, Y. Xue, Y.-M. Yan, K. Sun, *Catalysis Communications* **2015**, *67*, 78-82.
[8] Y. Liang, H. Wang, J. Zhou, Y. Li, J. Wang, T. Regier, H. Dai, *Journal of the American Chemical Society* **2012**, *134*, 3517-3523.
[9] H. Zhang, B. Chen, H. Jiang, X. Duan, Y. Zhu, C. Li, *Nanoscale* **2018**, *10*, 12991-12996.
[10] A. Aijaz, J. Masa, C. Rösler, W. Xia, P. Weide, A. J. R. Botz, R. A. Fischer, W. Schuhmann, M. Muhler, **2016**, *55*, 4087-4091.
[11] M.-R. Gao, X. Cao, Q. Gao, Y.-F. Xu, Y.-R. Zheng, J. Jiang, S.-H. Yu, *ACS Nano* **2014**, *8*, 3970-3978.
[12] A. Grimaud, K. J. May, C. E. Carlton, Y.-L. Lee, M. Risch, W. T. Hong, J. Zhou, Y. Shao-Horn, *Nature Communications* **2013**, *4*, 2439.
[13] B. S. Yeo, A. T. Bell, *Journal of the American Chemical Society* **2011**, *133*, 5587-5593.
[14] L. Xu, Y. Zou, Z. Xiao, S. Wang, *Journal of Energy Chemistry* **2019**, *35*, 24-29.
[15] R. Wei, M. Fang, G. Dong, C. Lan, L. Shu, H. Zhang, X. Bu, J. C. Ho, *ACS Applied Materials & Interfaces* **2018**, *10*, 7079-7086.
[16] L. Zhuang, L. Ge, Y. Yang, M. Li, Y. Jia, X. Yao, Z. Zhu, *Advanced Materials* **2017**, *29*, 1606793.
[17] aJ. Wang, R. Gao, D. Zhou, Z. Chen, Z. Wu, G. Schumacher, Z. Hu, X. Liu, *ACS Catalysis* **2017**, *7*, 6533-6541; bF.-C. Shen, Y. Wang, Y.-J. Tang, S.-L. Li, Y.-R. Wang, L.-Z. Dong, Y.-F. Li, Y. Xu, Y.-Q. Lan, *ACS Energy Letters* **2017**, *2*, 1327-1333.
[18] X. Wang, P. Sun, H. Lu, K. Tang, Q. Li, C. Wang, Z. Mao, T. Ali, C. Yan, *Small* **2019**, *15*, 1804886.
[19] M. Yang, Y. Li, Y. Yu, X. Liu, Z. Shi, Y. Xing, **2018**, *24*, 13002-13008.

[20] I. L. Júnior, J.-M. M. Millet, M. Aouine, M. do Carmo Rangel, *Applied Catalysis A: General* **2005**, *283*, 91-98.
[21] K. Fan, Y. Ji, H. Zou, J. Zhang, B. Zhu, H. Chen, Q. Daniel, Y. Luo, J. Yu, L. Sun, *Angew Chem Int Ed Engl* **2017**, *56*, 3289-3293.
[22] T. M. Masikhwa, J. K. Dangbegnon, A. Bello, M. J. Madito, D. Momodu, N. Manyala, *Journal of Physics and Chemistry of Solids* **2016**, *88*, 60-67.
[23] W. Wang, J. Xu, *ACS Applied Materials & Interfaces* **2015**, *7*, 415-421.
[24] K. Fan, H. Chen, Y. Ji, H. Huang, P. M. Claesson, Q. Daniel, B. Philippe, H. Rensmo, F. Li, Y. Luo, *Nature Communications* **2016**, *7*.
[25] J. Yang, H. Cheng, R. L. Frost, *Spectrochimica Acta Part A: Molecular and Biomolecular Spectroscopy* **2011**, *78*, 420-428.
[26] J. Zhang, W. Gao, M. Dou, F. Wang, J. Liu, Z. Li, J. Ji, *Analyst* **2015**, *140*, 1686-1692.
[27] S. Huanhuan, L. Hanfeng, M. Fangwang, W. Zhoucheng, *Angewandte Chemie* **2017**, *129*, 588-592.
[28] J. C., N. G. A., B. O., *physica status solidi (b)* **1997**, *201*, 319-326.
[29] S. Lee, *Solid State Ionics* **2003**, *165*, 111-116.
[30] L. Frost Ray, A. Henry Dermot, L. Weier Matt, W. Martens, *Journal of Raman Spectroscopy* **2006**, *37*, 722-732.
[31] C. Julien, M. Massot, C. Pérez-Vicente, *Materials Science and Engineering: B* **2000**, *75*, 6-12.
[32] aW. Li, X. Nie, X. Jiang, A. Zhang, F. Ding, M. Liu, Z. Liu, X. Guo, C. Song, *Applied Catalysis B: Environmental* **2018**, *220*, 397-408; bD. Klissurski, E. Uzunova, *Chemistry of Materials* **1991**, *3*, 1060-1063.
[33] A. Parmaliana, F. Arena, F. Frusteri, G. Martra, S. Coluccia, V. Sokolovskii, in *Studies in Surface Science and Catalysis, Vol. 110* (Eds.: R. K. Grasselli, S. T. Oyama, A. M. Gaffney, J. E. Lyons), Elsevier, **1997**, pp. 347-356.
[34] L. Wang, J. Zhu, X. Liu, *ACS Appl. Mater. Interfaces* **2019**, *11*, 22272-22277.
[35] J. Pritchard, L. Morris, D. Walsh, S. Sadasivan, H. Ménard, R. M. Bellabarba, M. T. Weller, R. P. Tooze, *Catalysis Letters* **2018**, *148*, 235-245.
[36] S. Li, S. Peng, L. Huang, X. Cui, A. M. Al-Enizi, G. Zheng, *ACS Applied Materials & Interfaces* **2016**, *8*, 20534-20539.
[37] C.-T. Wang, M.-T. Chen, D.-L. Lai, *Applied Surface Science* **2011**, *257*, 5109-5114.
[38] H. Liu, X. Liu, Z. Mao, Z. Zhao, X. Peng, J. Luo, X. Sun, *Journal of Power Sources* **2018**, *400*, 190-197.
[39] aW. G. Hardin, D. A. Slanac, X. Wang, S. Dai, K. P. Johnston, K. J. Stevenson, *The Journal of Physical Chemistry Letters* **2013**, *4*, 1254-1259; bJ. Suntivich, H. A. Gasteiger, N. Yabuuchi, H. Nakanishi, J. B. Goodenough, Y. Shao-Horn, *Nature Chemistry* **2011**, *3*, 546; cJ. Suntivich, K. J. May, H. A. Gasteiger, J. B. Goodenough, Y. Shao-Horn, **2011**, *334*, 1383-1385.
[40] Y. Zhan, G. Du, S. Yang, C. Xu, M. Lu, Z. Liu, J. Y. Lee, *ACS Applied Materials & Interfaces* **2015**, *7*, 12930-12936.
[41] X. Peng, L. Wang, L. Hu, Y. Li, B. Gao, H. Song, C. Huang, X. Zhang, J. Fu, K. Huo, P. K. Chu, *Nano Energy* **2017**, *34*, 1-7.
[42] M. Xing, L.-B. Kong, M.-C. Liu, L.-Y. Liu, L. Kang, Y.-C. Luo, *Journal of Materials Chemistry A* **2014**, *2*, 18435-18443.
[43] J. Zhang, B. Yuan, S. Cui, N. Zhang, J. Wei, X. Wang, D. Zhang, R. Zhang, Q. Huo, *Dalton Transactions* **2017**, *46*, 3295-3302.
[44] L. Liardet, X. Hu, *ACS Catalysis* **2018**, *8*, 644-650.

[45] aY. Sun, S. Gao, F. Lei, Y. Xie, *Chemical Society Reviews* **2015**, *44*, 623-636; bT. Maiyalagan, K. A. Jarvis, S. Therese, P. J. Ferreira, A. Manthiram, *Nature Communications* **2014**, *5*, 3949.
[46] aJ. Rosen, G. S. Hutchings, F. Jiao, *Journal of the American Chemical Society* **2013**, *135*, 4516-4521; bY. Sun, S. Gao, F. Lei, J. Liu, L. Liang, Y. Xie, *Chemical Science* **2014**, *5*, 3976-3982.
[47] M. S. Burke, M. G. Kast, L. Trotochaud, A. M. Smith, S. W. Boettcher, *Journal of the American Chemical Society* **2015**, *137*, 3638-3648.
[48] aM. S. Burke, L. J. Enman, A. S. Batchellor, S. Zou, S. W. Boettcher, *Chemistry of Materials* **2015**, *27*, 7549-7558; bL. Wang, C. Lin, F. Zhang, J. Jin, *ACS Nano* **2014**, *8*, 3724-3734.
[49] J. Haber, M. Witko, R. Tokarz, *Applied Catalysis A: General* **1997**, *157*, 3-22.
[50] J. Jiang, F. Sun, S. Zhou, W. Hu, H. Zhang, J. Dong, Z. Jiang, J. Zhao, J. Li, W. Yan, M. Wang, *Nature Communications* **2018**, *9*, 2885.
[51] T. Chun, Z. Rong, L. Wenbo, H. Liangbo, J. Xiue, A. A. M., S. Xuping, *Advanced Materials* **2017**, *29*, 1602441.